

# Quasinormal modes of a charged black hole with scalar hair

Wen-Di Guo<sup>ab\*</sup> and Qin Tan<sup>ab†</sup>

<sup>a</sup>Lanzhou Center for Theoretical Physics, Key Laboratory of Theoretical Physics of Gansu Province, School of Physical Science and Technology, Lanzhou University, Lanzhou 730000, People's Republic of China

<sup>b</sup>Institute of Theoretical Physics & Research Center of Gravitation, Lanzhou University, Lanzhou 730000, People's Republic of China

From a five-dimensional Einstein-Maxwell theory, Bah et al. constructed a singularity free topology star/black hole [Phys. Rev. Lett. 126, 151101 (2021)]. After the Klein-Kluza reduction, i.e., integrating the extra space dimension, it can obtain an effective four-dimensional static spherical charged black hole with scalar hair. In this paper, we study the quasinormal modes (QNMs) of the scalar field, electromagnetic field, and gravitational field on the background of this effective four-dimensional charged black hole. The radial parts of the perturbed fields all satisfy a Schrödinger-like equation. Using the asymptotic iteration method, we obtain the QNM frequencies semianalytically. For low overtone QNMs, the results obtained from the asymptotic iteration method and the Wentzel-Kramers-Brillouin approximation method agree well. In the null coordinates, the evolution of a Gaussian package is also studied. The QNM frequencies obtained by fitting the evolution data also agree well with the results obtained by the asymptotic iteration method.

PACS numbers:

## I. INTRODUCTION

In 2015, Laser Interferometer Gravitational-Wave Observatory (LIGO) and Virgo detected the gravitational wave of a binary black hole system [1]. This opens the window to gravitational wave astrophysics. After that, the Event Horizon Telescope (EHT) took the first picture of the supermassive black hole at the center of galaxy M87 in 2019 [2–7] and the picture of the black hole in our Milky Way in 2022 [8–13]. These enhanced our ability of testing fundamental physical problems. One of them is that does singularity exist [14, 15]? Searching for black hole alternatives has been attracted a lot of interest. Ultra-compact objects such as gravastars [16], boson stars [17], wormholes [18–21] have been constructed. More details can be seen in the review [22] and references therein. However, these models usually need some exotic matters and their UV origin is not clear. On the other hand, from string theory, the most important candidate which can unify quantum theory and gravity theory, some horizonless models have been constructed. One of them, fuzz ball, has smooth microstate geometry and it is similar to classical black hole up to Planck scale [23]. But constructing fuzz ball needs a lot of degrees of freedom, and it is difficult to study the astrophysical observations [24–26]. In order to alleviate these disadvantages, Bah and Heidmann proposed a topological star/black hole model which can be constructed from type-II B string theory and it is similar to classical black holes on macrostate geometries [27, 28]. So studying the astrophysical observations is not so difficult. They further analysed the

thermodynamic stability carefully of this solution [30]. Besides, the motion of a charged particle on the background of this topological star/black hole model has been studied [29]. Based on this solution, a four-dimensional static spherical charged black hole with scalar hair can be obtained by integrating the extra dimension [27, 28]. We will study the quasinormal modes (QNMs) of the scalar field, electromagnetic field and gravitational field on the background of this black hole in this paper.

Quasinormal modes are the characteristic modes of dissipative systems and have been playing important roles in a lot of physical areas. Classically, everything falling into the interior of the black hole can not escape, because of the event horizon, so black holes are dissipative systems. Quasinormal modes of black holes dominates the ringdown stage, the final stage of gravitational waves for a binary black hole merging system [32]. A big difference between the QNMs and normal modes is that the eigenfunctions of normal modes form a complete set, but the QNMs do not [33]. Besides, the eigenfunctions of QNMs are not normalizable [33]. Quasinormal modes have complex frequencies, the real parts are the vibration frequencies, and the imaginary parts are the inverse of the decay time scale of the perturbation. It is very important to study the QNMs of black holes. The mass and angular momentum can be inferred from the QNMs, and the no-hair theorem can also be tested through QNMs [35–37]. For horizonless compact objects, there could be echoes in the ringdown signal, which is the smoking gun of the existence of the horizonless compact objects [22, 38, 39]. One can also use the QNMs to constrain modified gravity theories [42–50]. It is also found the QNM spectrum is unstable under the small perturbation of the potential [40, 41]. Besides, the QNM frequencies can also partly reveal the stability of the background spacetime under small perturbations [51, 52]. In other physical systems, QNMs also play very important roles, for example, leaky reso-

\*guowd@lzu.edu.cn, Wen-Di Guo and Qin Tan are co-first authors of this paper.

†tanq19@lzu.edu.cn

nant cavities [53], and brane world models [54–56]. It has been studied widely [57–63].

In this paper, we will study the QNMs on the background of the four-dimensional static spherical black hole with scalar hair. The paper is organized as follows. In Sec. II, we give a brief review on the charged black hole with scalar hair and the KK reduction. In Sec. III, we study the small perturbation of scalar field, electromagnetic field and gravitational field. Expanding the perturbation fields in spherical harmonic function, we can derive the master equations of the perturbation. In Sec. IV, we compute the QNM frequencies using the asymptotic iteration method (AIM) and Wentzel-Kramers-Brillouin (WKB) approximation method, and the time evolution of a Gaussian package. Finally, we give the conclusions in Sec. V.

## II. THE CHARGED BLACK HOLE

The nonsingular black hole/topology star proposed by I. Bah and P. Hedmann [27, 28] started from the action of a five-dimensional Einstein-Maxwell theory

$$S = \int d^5x \sqrt{-\hat{g}} \left( \frac{1}{2\kappa_5^2} \hat{R} - \frac{1}{4} \hat{F}^{MN} \hat{F}_{MN} \right), \quad (1)$$

where  $\hat{F}_{MN}$  is the five-dimensional electromagnetic field tensor and  $\kappa_5$  is the five-dimensional gravitational constant. We use the hat to denote the five-dimensional quantities. And the capital Latin letters  $M, N, \dots$  are used to denote the five-dimensional coordinates. They considered a spherically symmetric metric [64]

$$ds^2 = -f_S(r)dt^2 + f_B(r)dy^2 + \frac{1}{f_S(r)f_B(r)}dr^2 + r^2d\theta^2 + r^2\sin^2\theta d\phi^2. \quad (2)$$

The extra dimension coordinate is denoted by  $y$ . The field strength of the magnetic field is

$$\hat{F} = P \sin\theta d\theta \wedge d\phi. \quad (3)$$

The solution can be solved as [64]

$$f_B(r) = 1 - \frac{r_B}{r}, \quad f_S(r) = 1 - \frac{r_S}{r}, \quad P = \pm \frac{1}{\kappa_5^2} \sqrt{\frac{3r_S r_B}{2}}. \quad (4)$$

Metric (2) is symmetric under the double rotation, which transforms the coordinate  $(t, y, r_S, r_B)$  to  $(iy, it, r_B, r_S)$ . The spacetime at  $r = r_S$  is a horizon, where  $f_S(r) = 0$ , and the spacetime at  $r = r_B$  is a degeneracy of the  $y$ -circle. Bah and Heidmann showed that there are smooth bubbles at  $r = r_B$  which ends the spacetime [27, 28]. The spacetime has two configurations. One is black string, when  $r_S \geq r_B$ , because the bubble hides behind the horizon. The other is topology star, when  $r_S < r_B$ , the horizon disappear because the spacetime ends at  $r = r_B$  [27, 28].

We rewrite the metric (2) as

$$ds_5^2 = e^{2\Phi} ds_4^2 + e^{-4\Phi} dy^2, \quad (5)$$

$$ds_4^2 = f_B^{\frac{1}{2}} \left( -f_S dt^2 + \frac{dr^2}{f_B f_S} + r^2 d\theta^2 + r^2 \sin^2\theta d\phi^2 \right) \quad (6)$$

where

$$e^{2\Phi} = f_B^{-1/2}, \quad (7)$$

and  $\Phi$  is a dilaton field. After the Kaluza-Klein reduction, i.e., integrating the extra dimension, we can obtain a four-dimensional Einstein-Maxwell-dilaton theory

$$S_4 = \int d^4x \sqrt{-g} \left( \frac{1}{2\kappa_4^2} R_4 - \frac{3}{\kappa_4^2} g^{\mu\nu} \partial_\mu \Phi \partial_\nu \Phi - 2\pi R_y e^{-2\Phi} F_{\mu\nu} F^{\mu\nu} \right), \quad (8)$$

where  $R_y$  is the radius of the extra dimension. We use the Greek letters  $\mu, \nu, \dots$  to label the four-dimensional coordinates. Here, the quantities without hat are constructed in four-dimensional spacetime. The four-dimensional gravitational constant is defined as

$$\kappa_4 = \frac{\kappa_5}{\sqrt{2\pi R_y}}. \quad (9)$$

We can solve the four-dimensional field strength of the magnetic field as

$$F = \pm \frac{1}{\kappa_4 \sqrt{2\pi R_y}} \sqrt{\frac{3r_B r_S}{2}} \sin\theta d\theta \wedge d\phi. \quad (10)$$

The ADM mass  $M$  and the magnetic charge  $Q_m$  can be solved as

$$M = 2\pi \left( \frac{2r_S + r_B}{\kappa_4^2} \right),$$

$$Q_m = \frac{1}{\kappa_4} \sqrt{\frac{3}{2}} r_B r_S. \quad (11)$$

Or, in terms of  $M$  and  $Q_m$

$$r_S^{(1)} = \frac{\kappa_4^2}{8\pi} (M - M_\Delta), \quad r_B^{(1)} = \frac{\kappa_4^2}{4\pi} (M + M_\Delta), \quad (12)$$

$$r_S^{(2)} = \frac{\kappa_4^2}{8\pi} (M + M_\Delta), \quad r_B^{(2)} = \frac{\kappa_4^2}{4\pi} (M - M_\Delta), \quad (13)$$

where  $M_\Delta^2 = M^2 - \left( \frac{8\pi Q_m}{\sqrt{3}\kappa_4} \right)^2$ . From solution (4) we know that, when  $r < r_B$ ,  $f_B^{1/2}$  becomes imaginary, and the metric is unphysical. So, the coordinate  $r$  can not smaller than  $r_B$ . Besides, the the black string scenario has Gregory-Laflamme instability [66]. However, the models with compact extra dimensions which will lead to a discrete KK mass spectrum could avoid the Gregory-Laflamme instability. Stotyn and Mann have demonstrated that, when  $R_y > \frac{4\sqrt{3}}{3} Q_m$ , solution (13) is stable. Note that, the spacetime at  $r = r_B$  is singular, so when  $r_S \geq r_B$  the metric (6) describes a charged black hole with scalar hair. We only study this case in this paper. Note that, the magnetically charged black holes have been studied in Refs. [67–69].

### III. PERTURBATION EQUATIONS

In this section, we analyse the linear perturbation equations of the scalar field, electromagnetic field, and gravitational field on the background of the charged black hole with scalar hair. For simplicity, we consider the three kinds of perturbed fields separately, that is to say, when one field is perturbed, the background of the other two fields are not affected. Although, usually the perturbations of the electromagnetic field and gravitational field should be coupled together for charged black holes.

#### A. Scalar field

We consider a free massless scalar field on this charged black hole background. The equation of motion for the scalar field is the Klein-Gordon equation

$$\frac{1}{\sqrt{-g}}\partial_\mu(\sqrt{-g}\partial^\mu\varphi) = 0. \quad (14)$$

Because of the spherical symmetry and time independence of the background, we can decompose the scalar field as

$$\varphi(t, r, \theta, \phi) = \sum_{l,m} e^{-i\omega t} f_B^{-1/4} \frac{1}{r} \psi_s(r) Y_{l,m}(\theta, \phi), \quad (15)$$

where  $Y_{l,m}$  is the spherical harmonics which satisfies

$$\Delta Y_{l,m} = -l(l+1)Y_{l,m}, \quad (16)$$

with  $\Delta$  the Laplace-Beltrami operator. Substituting this into Eq. (14), we obtain the radial part of the perturbation equation for the scalar field

$$f_S^2 f_B \psi_s'' + f_S (f_S' f_B + \frac{1}{2} f_B' f_S) \psi_s' + (\omega^2 - V_s(r)) \psi_s = 0, \quad (17)$$

where

$$V_s(r) = f_S \left( \frac{l(l+1)}{r^2} + \frac{1}{4} f_S f_B'' + f_B' f_S' - \frac{f_S f_B'^2}{4f_B} \right) + \frac{f_S}{r} (f_S f_B' + f_B f_S') \quad (18)$$

is the effective potential for the scalar field. Hereafter, we use prime to denote the derivative with respect to the coordinate  $r$ . In order to obtain the Schrödinger-like equation, we need the tortoise coordinate  $r_*$ , which can be obtained from the following relation

$$dr_* = \frac{1}{\sqrt{f_B f_S}} dr. \quad (19)$$

In this way, Eq. (17) can be written as

$$\frac{d^2\psi(r_*)}{dr_*^2} + (\omega^2 - V_s(r_*))\psi(r_*) = 0. \quad (20)$$

#### B. Electromagnetic field

For an electromagnetic field, the Maxwell equation is given by

$$\frac{1}{\sqrt{-g}}\partial_\mu(\sqrt{-g}\tilde{F}^{\mu\nu}) = 0, \quad (21)$$

where  $\tilde{F}_{\mu\nu} = \partial_\mu\tilde{A}_\nu - \partial_\nu\tilde{A}_\mu$  is the field strength tensor of the perturbed electromagnetic field  $\tilde{A}_\mu$ . To separate the perturbed electromagnetic field, we need the vectorial spherical harmonics which are defined as [70–72]

$$(V_{l,m}^1)_a = \partial_a Y_{l,m}(\theta, \phi), \quad (22)$$

$$(V_{l,m}^2)_a = \gamma^{bc}\epsilon_{ac}\partial_b Y_{l,m}(\theta, \phi). \quad (23)$$

Here, the Latin letters  $a, b, c$  denote the angular coordinates  $\theta$  and  $\phi$ ,  $\gamma$  is the induced metric on the sphere with radius 1, and  $\epsilon$  is the totally antisymmetric tensor in two dimensions. Note that,  $(V_{l,m}^1)_a$  and  $(V_{l,m}^2)_a$  behave differently under the space inversion, i.e.,  $(\theta, \phi) \rightarrow (\pi - \theta, \pi + \phi)$ .  $(V_{l,m}^1)_a$  is even or polar, that is, it acquires a factor  $(-1)^l$  under space inversion,  $(V_{l,m}^2)_a$  is odd or axial, that is, it acquires a factor  $(-1)^{l+1}$  under space inversion. Thus, the perturbed electromagnetic field  $\tilde{A}_\mu$  can be decomposed as

$$\tilde{A}_\mu(t, r, \theta, \phi) = \sum_{l,m} e^{-i\omega t} \begin{bmatrix} 0 \\ 0 \\ \frac{\psi_v(r)}{\sin\theta} \frac{\partial Y_{l,m}}{\partial\phi} \\ -\psi_v(r) \sin\theta \frac{\partial Y_{l,m}}{\partial\theta} \end{bmatrix} + \sum_{l,m} e^{-i\omega t} \begin{bmatrix} h_1(r) Y_{l,m} \\ h_2(r) Y_{l,m} \\ h_3(r) \frac{\partial Y_{l,m}}{\partial\theta} \\ h_3(r) \frac{\partial Y_{l,m}}{\partial\phi} \end{bmatrix}. \quad (24)$$

Owing to the spherical symmetry of the background metric, the perturbation equations will not mix polar and axial contributions. Besides, the axial part and the polar part will contribute to the same result [70, 71]. So, we only need to deal with the axial part. Substituting the background metric (6) into the Maxwell equation (21), we obtain the perturbation equation for the radial part  $\psi_v$

$$f_S^2 f_B \psi_v'' + f_S (f_S' f_B + \frac{1}{2} f_B' f_S) \psi_v' + (\omega^2 - V_v(r)) \psi_v = 0, \quad (25)$$

where the effective potential is

$$V_v(r) = \frac{f_S(r)l(l+1)}{r^2}, \quad (26)$$

which does not depend on the parameter  $r_B$ . But the effective potential depends on the parameter  $r_S$  which is related to the magnetic charge  $Q_m$ . Using the tortoise coordinate  $r_*$ , the perturbation equation can also be transformed into a Schrödinger-like form. From Eq. (19) we know that, the tortoise coordinate  $r_*$  depends on the parameter  $r_B$ , so the QNMs will also be affected by the parameter  $r_B$ .

### C. Gravitational field

Considering a perturbation on the background metric (6), the perturbed metric is

$$\bar{g}_{\mu\nu} = g_{\mu\nu} + h_{\mu\nu}, \quad (27)$$

where  $h_{\mu\nu}$  is the perturbation. The separation of the perturbation for the gravitational field is more complicated. Besides the vectorial spherical harmonics, we also need the tensorial harmonics, which are defined as [73]

$$(T_{l,m}^1)_{ab} = (Y_{l,m})_{;ab}, \quad (28)$$

$$(T_{l,m}^2)_{ab} = Y_{l,m}\gamma_{ab}, \quad (29)$$

$$(T_{l,m}^3)_{ab} = \frac{1}{2} [\epsilon_a^c (Y_{l,m})_{;cb} + \epsilon_b^c (Y_{l,m})_{;ca}], \quad (30)$$

where the semicolon denotes the covariant derivative on the sphere. Among them,  $T_{l,m}^3$  is odd under the space inversion, the other two are even. Based on the principle of general covariance, the theory should keep covariant under infinitesimal coordinate transformation. Thus, we can choose a specific gauge to simplify the problem. In the Regge-Wheeler gauge [73], the perturbation  $h_{\mu\nu}$  can be written as

$$h_{\mu\nu} = \sum_l e^{-i\omega t} \begin{bmatrix} 0 & 0 & 0 & h_0(r) \\ 0 & 0 & 0 & h_1(r) \\ 0 & 0 & 0 & 0 \\ h_0(r) & h_1(r) & 0 & 0 \end{bmatrix} \sin\theta \partial_\theta Y_{l,0}(\theta) \quad (31)$$

for the odd parity, and

$$h_{\mu\nu} = \sum_l e^{-i\omega t} \begin{bmatrix} H_0(r) & H_1(r) & 0 & 0 \\ H_1(r) & H_2(r) & 0 & 0 \\ 0 & 0 & r^2 K(r) & 0 \\ 0 & 0 & 0 & r^2 K(r) \sin^2\theta \end{bmatrix} Y_{l,0}(\theta) \quad (32)$$

for the even parity. Note that, we have chosen  $m = 0$  for simplicity, because the perturbation equations do not depend on the value of  $m$  [73]. For the Schwarzschild black hole, the odd parity and the even parity have the same QNM spectrum [74], but other black holes may not exist this property. Anyway, for simplicity, we just study the odd parity in this paper. Substituting the decomposition into Einstein's equation, and after some algebraic operations, the perturbation equations for the odd parity perturbation can be combined into a single equation for the variable  $\psi_g$ , which is defined as

$$\psi_g(r) = \frac{f_B^{1/4}(r) f_S(r)}{r} h_1(r). \quad (33)$$

The variable  $\psi_g$  satisfies the Schrödinger-like equation (20), with the effective potential

$$V_g(r) = f_S \left( \frac{3}{4} f_B' f_S' + f_B f_S'' - \frac{f_B f_S'}{r} + \frac{l(l+1)}{r^2} \right) - f_S^2 \left( \frac{9 f_B'^2}{16 f_B} - \frac{3 f_B''}{4} \right). \quad (34)$$

The effective potential plays an important role on determining the value of QNMs. We plot the effective potentials for scalar field, electromagnetic field, and gravitational field in Fig. 1. All of the effective potentials approach to zero at the horizon and infinity, which is similar to that of the Schwarzschild black hole. Besides, the effective potentials for the scalar field and the gravitational field depend on the parameter  $r_B$ .

## IV. COMPUTING QNMS

In this section we will solve the QNMs of the charged black hole with scalar field both in frequency domain and time domain. And we will compare the results by the two methods.

### A. Solving frequency

First, we solve the frequencies of QNMs for the three kinds of fields using the AIM and WKB approximation method. Now, we give a brief review on the AIM.

Considering a homogeneous linear second-order differential equation

$$\chi''(x) = \lambda_0(x)\chi'(x) + s_0(x)\chi(x), \quad (35)$$

where  $\lambda_0(x)$  and  $s_0(x)$  are smooth functions. Based on the symmetric structure of the right-hand of Eq. (35), we can find a general solution of this equation [75]. Differentiating Eq. (35) with respect to the variable  $x$ , we obtain

$$\chi'''(x) = \lambda_1(x)\chi'(x) + s_1(x)\chi(x), \quad (36)$$

where

$$\begin{aligned} \lambda_1(x) &= \lambda_0'(x) + s_0(x) + (\lambda_0)^2, \\ s_1(x) &= s_0'(x) + s_0(x)\lambda_0(x). \end{aligned} \quad (37)$$

Differentiating Eq. (36) with respect to  $x$  again, we find that

$$\chi''''(x) = \lambda_2(x)\chi'(x) + s_2(x)\chi(x), \quad (38)$$

where

$$\begin{aligned} \lambda_2(x) &= \lambda_1'(x) + s_1(x) + \lambda_0\lambda_1, \\ s_2(x) &= s_1'(x) + s_0(x)\lambda_1(x). \end{aligned} \quad (39)$$

Continue this process, the  $(n+1)$ -th and  $(n+2)$ -th derivatives give us the following relations

$$\begin{aligned} \lambda_n(x) &= \lambda_{n-1}'(x) + s_{n-1}(x) + \lambda_0(x)\lambda_{n-1}(x), \\ s_n(x) &= s_{n-1}'(x) + s_0(x)\lambda_{n-1}(x). \end{aligned} \quad (40)$$

When  $n$  is sufficiently large, the asymptotic aspect can be introduced as

$$\frac{s_n(x)}{\lambda_n(x)} = \frac{s_{n-1}(x)}{\lambda_{n-1}(x)}. \quad (41)$$

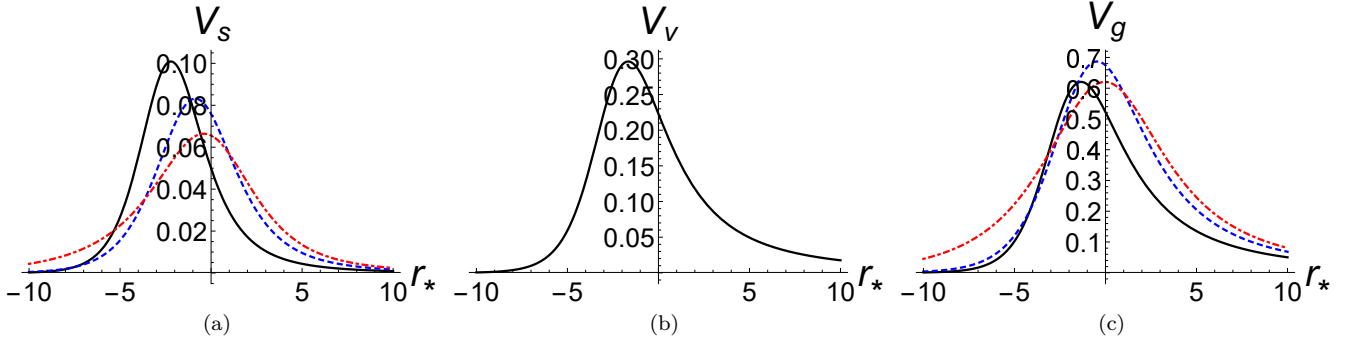


FIG. 1: The effective potentials in the tortoise coordinate  $r_*$ . The parameter  $r_B$  is set to  $r_B = 0.1r_S$  (the black solid lines),  $r_B = 0.5r_S$  (the blue dashed lines), and  $r_B = 0.9r_S$  (the red dot dashed lines). (a) The scalar field with  $l = 0$ . (b) The electromagnetic field with  $l = 1$ . (c) The gravitational field with  $l = 2$ .

Then, the QNMs can be obtained from the “quantization condition”

$$s_n \lambda_{n-1} - s_{n-1} \lambda_n = 0. \quad (42)$$

This is equivalent to give the iteration number  $n$  a truncation. This method is good, but one needs to differentiate the  $s(x)$  and  $\lambda(x)$  terms for each iteration, which may bring problems for numerical precision. To make the process more efficient, Cho et al. [76] improved this method. The improved method does not need to take derivatives at each step, which greatly improves the accuracy and the speed. What they do is expanding the  $\lambda_n$  and  $s_n$  in a Taylor series around a fix point  $\xi$ ,

$$\begin{aligned} \lambda_n(x) &= \sum_{i=0}^{\infty} c_n^i (x - \xi)^i, \\ s_n(x) &= \sum_{i=0}^{\infty} d_n^i (x - \xi)^i, \end{aligned} \quad (43)$$

where  $c_n^i$  and  $d_n^i$  are the  $i$ -th Taylor coefficients of  $\lambda_n$  and  $s_n$ , respectively. Using these expressions, one can obtain a set of recursion relations:

$$\begin{aligned} c_n^i &= (i+1)c_{n-1}^{i+1} + d_{n-1}^i + \sum_{k=0}^i c_0^k c_{n-1}^{i-k}, \\ d_n^i &= (i+1)d_{n-1}^{i+1} + \sum_{k=0}^i d_0^k c_{n-1}^{i-k}. \end{aligned} \quad (44)$$

Thus, the “quantization condition” can be reexpressed in terms of the coefficients as

$$d_n^0 c_{n-1}^0 - d_{n-1}^0 c_n^0 = 0. \quad (45)$$

The boundary conditions are pure ingoing waves at the event horizon

$$\psi \sim e^{-i\omega r_*}, \quad r_* \rightarrow -\infty, \quad (46)$$

and pure outgoing waves at spatial infinity

$$\psi \sim e^{i\omega r_*}, \quad r_* \rightarrow +\infty. \quad (47)$$

It is helpful to transform the infinity to be finite, so we perform the following coordinate transformation

$$u = 1 - \frac{r_S}{r}, \quad (48)$$

such that, the range of  $u$  is  $0 \leq u < 1$ . The boundary conditions in terms of  $u$  are

$$\psi(u) = \left( \frac{-2(r_S - r_B) + 2\sqrt{r_S - r_B}}{r_S^{5/2} u} \right)^{i\omega r_S^{3/2} / \sqrt{r_S - r_B}} \quad (49)$$

at the horizon, i.e.,  $u = 0$ , and

$$\psi(u) = e^{i\omega(r_S/(1-u) + (r_S + r_B)/2)} \left( \frac{4r_S}{1-u} - r_B \right)^{i\omega} \quad (50)$$

at infinity, i.e.,  $u \rightarrow 1$ . Thus, we can define

$$\begin{aligned} \psi(u) &= \left( \frac{-2(r_S - r_B) + 2\sqrt{r_S - r_B}}{r_S^{5/2} u} \right)^{i\omega r_S^{3/2} / \sqrt{r_S - r_B}} \\ &\times \left( \frac{4r_S}{1-u} - r_B \right)^{i\omega} e^{i\omega \left( \frac{r_S}{1-u} + (r_S + \frac{r_B}{2}) \right)} \chi(u). \end{aligned} \quad (51)$$

Then, the perturbation equations can be rewritten as

$$\chi''(u) = \lambda_0(u)\chi'(u) + s_0(u)\chi \quad (52)$$

where  $\lambda_0$  and  $s_0$  are functions of  $u$  depending on the effective potential. The functions  $\lambda_0$  and  $s_0$  are complicated, so we do not show them explicitly. The first twenty modes for the scalar field, electromagnetic field, and gravitational field are shown in Fig. 2. The WKB method is powerful on solving frequencies of low overtone QNMs. We compare the results obtained by the AIM and by the WKB method in Tables I, II, III for the scalar field, electromagnetic field, and gravitational field, respectively. We find that, for low overtone QNMs, the results obtained through the AIM are in good agreement with that of obtained by the WKB method. When the



multipole number  $l$  increases, the real parts of the QNM frequencies change more apparently than the imaginary parts, which can be seen from Fig. 2 and Tables I, II, III. Note that,  $r_B = 0.5r_S$  is equivalent to  $Q_m = \frac{2\sqrt{2}}{3}\bar{M}$ , where  $\bar{M} \equiv \frac{\sqrt{3}\kappa_4}{8\pi}M$ .

$l$	$n$	AIM		WKB	
		$\text{Re}(\omega r_S)$	$\text{Im}(\omega r_S)$	$\text{Re}(\omega r_S)$	$\text{Im}(\omega r_S)$
0	0	0.220856	-0.166592	0.219664	-0.166443
	1	0.186884	-0.534457	0.193004	-0.537457
1	0	0.586476	-0.158533	0.586679	-0.158525
	1	0.554754	-0.488295	0.556358	-0.487138
2	0	0.967669	-0.157641	0.967666	-0.157648
	1	0.946096	-0.478040	0.946082	-0.478076

TABLE I: Frequencies of low overtone QNMs for the scalar field. The parameter  $r_B$  is set to  $r_B = 0.5r_S$ .

$l$	$n$	AIM		WKB	
		$\text{Re}(\omega r_S)$	$\text{Im}(\omega r_S)$	$\text{Re}(\omega r_S)$	$\text{Im}(\omega r_S)$
1	0	0.513377	-0.152855	0.513302	-0.153142
	1	0.476438	-0.474101	0.476701	-0.537457
2	0	0.924716	-0.155637	0.924714	-0.155649
	1	0.901934	-0.472399	0.901941	-0.472447
3	0	1.32049	-0.156374	1.32049	-0.156375
	1	1.30408	-0.471908	1.30408	-0.471914

TABLE II: Frequencies of low overtone QNMs for the electromagnetic field. The parameter  $r_B$  is set to  $r_B = 0.5r_S$ .

$l$	$n$	AIM		WKB	
		$\text{Re}(\omega r_S)$	$\text{Im}(\omega r_S)$	$\text{Re}(\omega r_S)$	$\text{Im}(\omega r_S)$
2	0	0.810272	-0.147554	0.810467	-0.147398
	1	0.785979	-0.449209	0.787063	-0.447841
3	0	1.24218	-0.152877	1.24220	-0.152875
	1	1.22506	-0.461665	1.22529	-0.461580
4	0	1.65149	-0.154694	1.65149	-0.154694
	1	1.63833	-0.465851	1.63831	-0.465856

TABLE III: Frequencies of low overtone QNMs for the gravitational field. The parameter  $r_B$  is set to  $r_B = 0.5r_S$ .

From Eq. (13) we know that, the mass  $M$  and the magnetic charge  $Q_m$  are closely related to the parameter  $r_B$  and  $r_S$ . When we fix the mass  $M$  and increase the magnetic charge  $Q_m$ , then  $r_S$  will decrease and  $r_B$  will increase. So the effect of the magnetic charge  $Q_m$  on the QNMs can be obtained through qualitatively analyse the effect of the parameter  $r_B$  on the QNMs. We study the effect of the parameter  $r_B$  on the fundamental QNMs for the three kinds of perturbed fields. The range of the parameter  $r_B$  is  $0 \leq r_B \leq 0.5r_S$ . It is equivalent that  $0 \leq Q_m \leq \frac{2\sqrt{2}}{3}\bar{M}$ . We find that the real parts of the overtone QNMs' frequencies for scalar field and vector field approximately increase linearly with  $r_B$ ,

while the absolute value of the imaginary parts approximately decrease linearly with  $r_B$ , which can be seen from Figs. 3(a)-3(d). As for the gravitational field, both the real parts and the absolute value of the imaginary parts of the overtone QNM frequencies change slightly with  $r_B$  for smaller  $r_B$ , after a short decrease stage, then they increase rapidly with  $r_B$ .

## B. Time evolution

In order to intuitively show the evolution of the perturbed field, we study the QNMs in the time domain, i.e., do not use the ansatz  $\psi \propto e^{-i\omega t}$ . Using the null coordinates  $u = t - r_*$  and  $v = t + r_*$ , the perturbation equations can be written in the following form

$$4\frac{\partial^2 \Phi_{s,v,g}}{\partial u \partial v} + V_{s,v,g}(r_*)\Phi_{s,v,g} = 0. \quad (53)$$

We choose the initial data as a Gaussian package

$$\begin{aligned} \Phi(0, v) &= e^{-\frac{(v-v_c)^2}{2\sigma^2}}, \\ \Phi(u, 0) &= 0. \end{aligned} \quad (54)$$

We choose the package located at  $v_c = 10r_S$ , with the width  $\sigma = 1r_S$ . The evolution ranges are  $(0, 200r_S)$ , and the results are extracted at  $r_* = 20r_S$ . The results are shown in Fig. 4. By fitting the evolution data, we can also obtain the QNM's frequency. For example, the frequency by fitting the evolution data of the electromagnetic field is  $0.512894 - 0.152494i$ , which agrees with the result by the AIM  $0.513377 - 0.152855i$  well. Although the fundamental QNM dominates the evolution of the perturbation, the evolution data are the superpositions of all the QNMs, so this result is good. All three methods obtain the same results enhance the credibility of the results.

## V. CONCLUSIONS

Through the KK reduction, the five-dimensional Einstein-Maxwell theory reduces to a four-dimensional Einstein-Maxwell-dilaton theory which supports a spherically static charged black hole solution. We studied the linear perturbation equations of scalar field, electromagnetic field, and gravitational field on this spherically static charged black hole background. Because of the spherical symmetry of the background, the radial parts of the perturbed fields can be decomposed from the angular parts. Using the tortoise coordinate  $r_*$ , every perturbation equation can be written into a Schrödinger-like form. The effective potentials for the scalar field, electromagnetic field, and gravitational field are shown in Fig. 1. From this figure we can see that, the effective potentials, except for that of the electromagnetic field, depend on the parameter  $r_B$ .

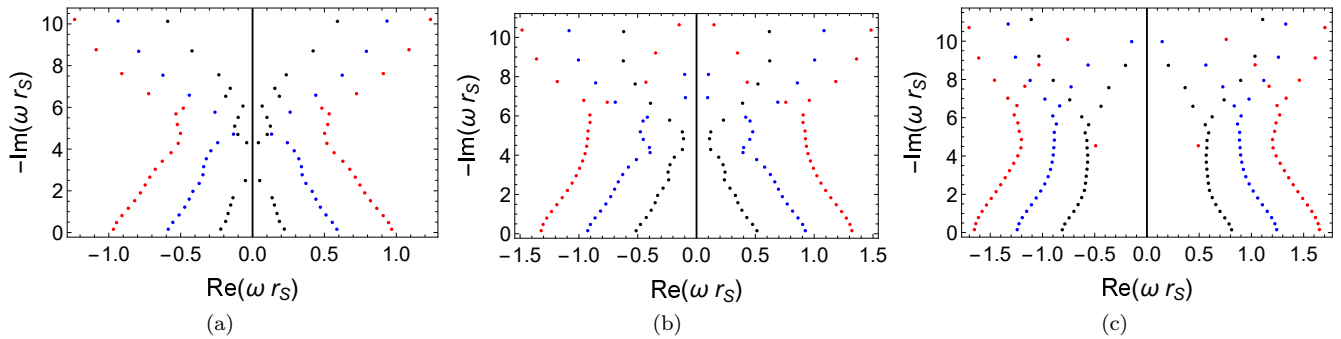


FIG. 2: The first twenty QNMs for this charged black hole with scalar hair. The parameter  $r_B$  is set to  $r_B = 0.5r_S$ . (a) QNMs for the scalar field with  $l = 0$  (the black dots),  $l = 1$  (the blue dots),  $l = 2$  (the red dots). (b) QNMs for the electromagnetic field with  $l = 1$  (the black dots),  $l = 2$  (the blue dots),  $l = 3$  (the red dots). (c) QNMs for the gravitational field with  $l = 2$  (the black dots),  $l = 3$  (the blue dots),  $l = 4$  (the red dots).

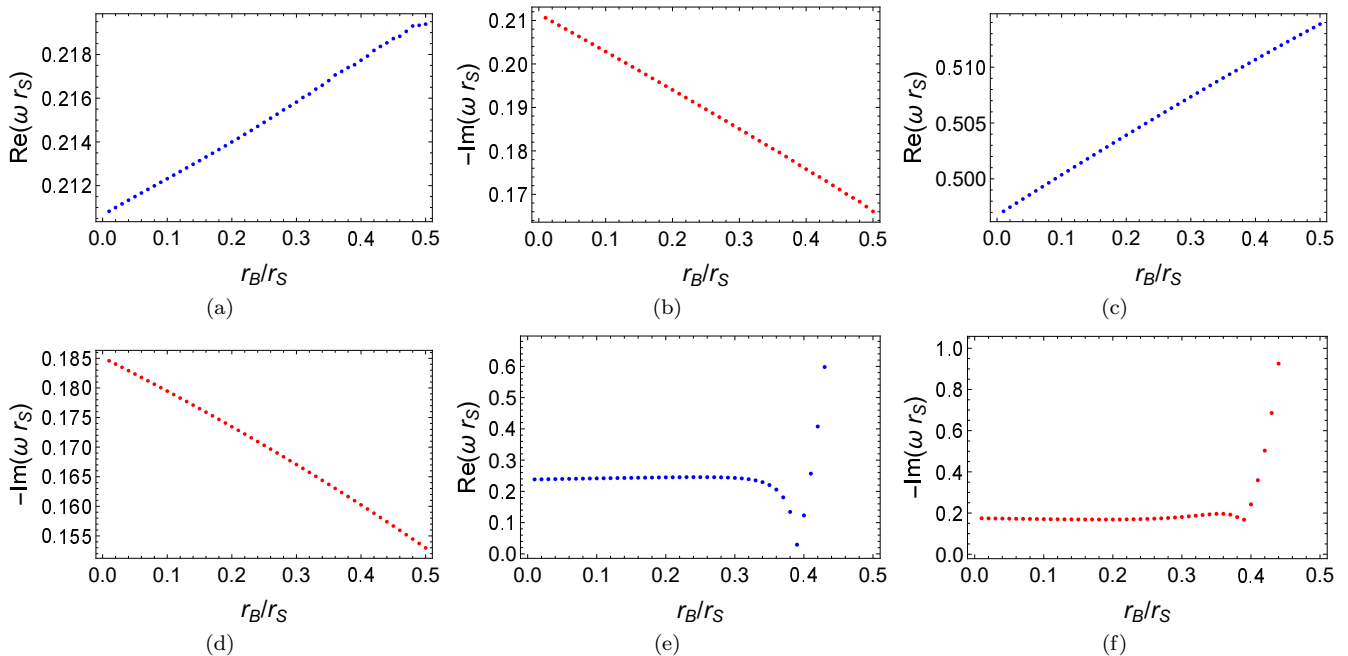


FIG. 3: The effect of the parameter  $r_B$  on the frequencies of fundamental QNMs. (a) Real parts of frequencies for the scalar field with  $l = 0$ . (b) Imaginary parts of frequencies for the scalar field with  $l = 0$ . (c) Real parts of frequencies for the electromagnetic field with  $l = 1$ . (d) Imaginary parts of frequencies for the electromagnetic field with  $l = 1$ . (e) Real parts of frequencies for the gravitational field with  $l = 2$ . (f) Imaginary parts of frequencies for the gravitational field with  $l = 2$ .

Using the AIM we computed the QNM frequencies for the three kinds of perturbed fields. As the multipole number  $l$  increases, the real parts of the QNM frequencies change more apparently than the imaginary parts, which can be seen from Fig. 2 and Tables I, II, III. We also compared the results obtained from the AIM and WKB method, and found that, for low overtone QNMs, the results obtained through AIM are in good agreement with that of obtained by WKB method. The effect of the parameter  $r_B$  were also studied. Using the null coordinates  $u$  and  $v$ , the evolution of a Gaussian package

was also investigated. The results showed that, the QNM frequencies obtained by fitting the evolution data agree well with the results by the AIM.

Note that, we only studied the QNMs for the charged black hole. For the topological star, there is no event horizon, so the ingoing boundary condition can not be imposed. Thus, it should be treated separately. We will study this in the future.

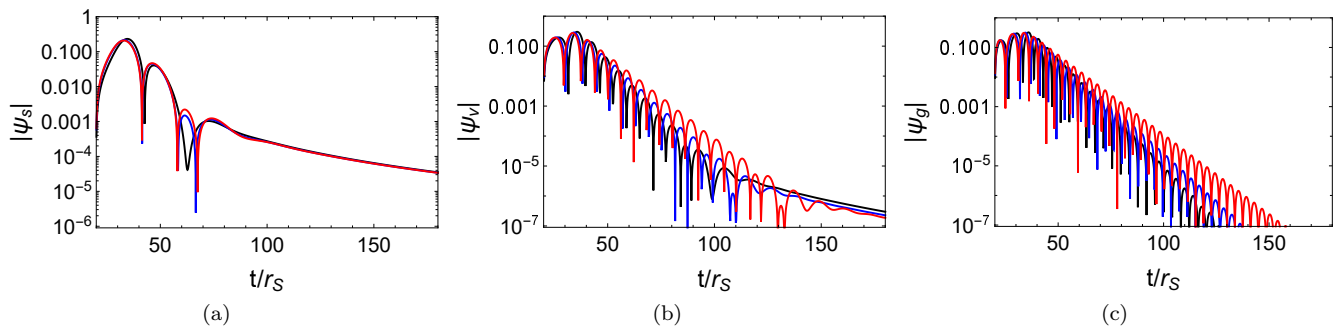


FIG. 4: Time evolution of the Gauss package extracted at  $r_* = 20$ . The parameter  $r_B$  is set as  $r_B = 0.2r_s$  (the black lines),  $r_B = 0.5r_s$  (the blue lines), and  $r_B = 0.8r_s$  (the red lines). (a) Time evolution of the scalar field with  $l = 0$ . (b) Time evolution of the electromagnetic field with  $l = 1$ . (c) Time evolution of the gravitational field with  $l = 2$ .

## VI. ACKNOWLEDGMENTS

This work was supported by National Key Research and Development Program of China (Grant No. 2020YFC2201503), the National Natural Science Foundation of China (Grants No. 12205129, No. 12147166,

No. 11875151, No. 12075103, and No. 12247101), the China Postdoctoral Science Foundation (Grant No. 2021M701529), the 111 Project (Grant No. B20063), and Lanzhou City's scientific research funding subsidy to Lanzhou University.

- 
- [1] LIGO Collaboration and Virgo Collaboration, *Observation of gravitational waves from a binary black hole merger*, *Phys. Rev. Lett.* **116**, 061102 (2016), [1602.03837].
- [2] EHT Collaboration, *First M87 event horizon telescope results. I. the shadow of the supermassive black hole*, *Astrophys. J. Lett.* **875**, L1 (2019), [1906.11238].
- [3] EHT Collaboration, *First M87 event horizon telescope results. II. array and instrumentation*, *Astrophys. J. Lett.* **875**, L2 (2019), [1906.11239].
- [4] EHT Collaboration, *First M87 event horizon telescope results. III. data processing and calibration*, *Astrophys. J. Lett.* **875**, L3 (2019), [1906.11240].
- [5] EHT Collaboration, *First M87 event horizon telescope results. IV. imaging the central supermassive black hole*, *Astrophys. J. Lett.* **875**, L4 (2019), [1906.11241].
- [6] EHT Collaboration, *First M87 event horizon telescope results. V. physical origin of the asymmetric ring*, *Astrophys. J. Lett.* **875**, L5 (2019), [1906.11242].
- [7] EHT Collaboration, *First M87 event horizon telescope results. VI. the shadow and mass of the central black hole*, *Astrophys. J. Lett.* **875**, L6 (2019), [1906.11243].
- [8] EHT Collaboration, *First Sagittarius A\* Event Horizon Telescope Results. I. The Shadow of the Supermassive Black Hole in the Center of the Milky Way*, *Astrophys. J. Lett.* **930**, L12 (2022).
- [9] EHT Collaboration, *First Sagittarius A\* Event Horizon Telescope Results. II. EHT and Multiwavelength Observations, Data Processing, and Calibration*, *Astrophys. J. Lett.* **930**, L13 (2022).
- [10] EHT Collaboration, *First Sagittarius A\* Event Horizon Telescope Results. III. Imaging of the Galactic Center Supermassive Black Hole*, *Astrophys. J. Lett.* **930**, L14 (2022).
- [11] EHT Collaboration, *First Sagittarius A\* Event Horizon Telescope Results. IV. Variability, Morphology, and Black Hole Mass*, *Astrophys. J. Lett.* **930**, L15 (2022).
- [12] EHT Collaboration, *First Sagittarius A\* Event Horizon Telescope Results. V. Testing Astrophysical Models of the Galactic Center Black Hole*, *Astrophys. J. Lett.* **930**, L16 (2022).
- [13] EHT Collaboration, *First Sagittarius A\* Event Horizon Telescope Results. VI. Testing the Black Hole Metric*, *Astrophys. J. Lett.* **930**, L17 (2022).
- [14] E. Berti, E. Barausse, V. Cardoso, L. Gualtieri, P. Pani, U. Sperhake et al., *Testing general relativity with present and future astrophysical observations*, *Class. Quantum Grav.* **32**, 243001 (2015), [1501.07274].
- [15] V. Cardoso, E. Franzin, and P. Pani, *Is the gravitational-wave ringdown a probe of the event horizon?* *Phys. Rev. Lett.* **116**, 171101 (2016), [1602.07309].
- [16] P. O. Mazur and E. Mottola, *Gravitational condensate stars: An alternative to black holes*, [gr-qc/0109035].
- [17] F. E. Schunck and E. W. Mielke, *Topical review: General relativistic boson stars*, *Class. Quant. Grav.* **20**, R301 (2003), [0801.0307].
- [18] S. N. Solodukhin, *Restoring unitarity in BTZ black hole*, *Phys. Rev. D* **71**, 064006 (2005), [hep-th/0501053].
- [19] D.-C. Dai and D. Stojkovic, *Observing a Wormhole*, *Phys. Rev. D* **100**, 083513 (2019), [1910.00429].
- [20] J. H. Simonetti, M. J. Kavic, D. Minic, D. Stojkovic, and D.-C. Da, *Sensitive searches for wormholes*, *Phys. Rev. D* **104**, L081502 (2021), [2007.12184].
- [21] C. Bambi and D. Stojkovic, *Astrophysical Wormholes*, *Universe* **7**, 136 (2021), [2105.00881].
- [22] V. Cardoso and P. Pani, *Testing the nature of dark compact objects: a status report*, *Living Rev. Relativ.* **22**, 4 (2019), [1904.05363].



- [23] G. W. Gibbons and N. P. Warner, *Global structure of five-dimensional BPS fuzzballs*, *Class. Quant. Grav.* **31**, 025016 (2014), [[1305.0957](#)].
- [24] I. Bena, F. Eperon, P. Heidmann, and N. P. Warner, *The great escape: Tunneling out of microstate geometries*, *JHEP* **04**, 112 (2021), [[2005.11323](#)].
- [25] I. Bena and D. R. Mayerson, *A new window into black holes*, *Phys. Rev. Lett.* **125**, 221602 (2020), [[2006.10750](#)].
- [26] I. Bena and D. R. Mayerson, *Black holes lessons from multipole ratios*, *JHEP* **03**, 114 (2021), [[2007.09152](#)].
- [27] I. Bah and P. Heidmann, *Topological stars and black holes*, *Phys. Rev. Lett.* **126**, 151101 (2021), [[2011.08851](#)].
- [28] I. Bah and P. Heidmann, *Topological stars, black holes and generalized charged weyl solutions*, [[2012.13407](#)].
- [29] Y.-K. Lim, *Motion of charged particles around a magnetic black hole/topological star with a compact extra dimension*, *Phys. Rev. D* **103**, 084044 (2021), [[2102.08531](#)].
- [30] I. Bah, A. Dey, and P. Heidmann *Stability of topological solitons, and black string to bubble transition*, *JHEP* **04**, 168 (2022), [[2112.11474](#)].
- [31] W.-D. Guo, S. -W. Wei, and Y.-X. Liu *Shadow of a charged black hole with scalar hair*, [[2203.13477](#)].
- [32] E. Berti, V. Cardoso, J. A. Gonzalez, and U. Sperhake, *Mining information from binary black hole mergers: A Comparison of estimation methods for complex exponentials in noise*, *Phys. Rev. D* **75**, 124017 (2007), [[gr-qc/0701086](#)].
- [33] H. P. Nollert and R. H. Price, *Quantifying excitations of quasinormal mode systems*, *J. Math. Phys.* **40**, 980 (1999), [[gr-qc/9810074](#)].
- [34] F. Echeverria, *Gravitational Wave Measurements of the Mass and Angular Momentum of a Black Hole*, *Phys. Rev. D* **40**, 3194 (1989).
- [35] E. Berti, V. Cardoso, and C. M. Will, *On gravitational-wave spectroscopy of massive black holes with the space interferometer LISA*, *Phys. Rev. D* **73**, 064030 (2006), [[gr-qc/0512160](#)].
- [36] E. Berti, J. Cardoso, V. Cardoso, and M. Cavaglia, *Matched-filtering and parameter estimation of ringdown waveforms*, *Phys. Rev. D* **76**, 104044 (2007), [[0707.1202](#)].
- [37] M. Isi, M. Giesler, W. M. Farr, M. A. Scheel, and S. A. Teukolsky, *Testing the no-hair theorem with GW150914*, *Phys. Rev. Lett.* **123**, 111102 (2019), [[1905.00869](#)].
- [38] V. Cardoso, E. Franzin, and P. Pani, *Is the gravitational-wave ringdown a probe of the event horizon?*, *Phys. Rev. Lett.* **116**, 171101 (2016), [[1602.07309](#)].
- [39] V. Cardoso and P. Pani, *Tests for the existence of black holes through gravitational wave echoes*, *Nature Astron.* **1**, 586 (2017), [[1709.01525](#)].
- [40] J. Jaramillo, R. P. Macedo, and L. A. Sheikh, *Pseudospectrum and Black Hole Quasinormal Mode Instability*, *Phys. Rev. X* **11**, 031003 (2021), [[2004.06434](#)].
- [41] M. H. Cheung, K. Destounis, R. P. Macedo, E. Berti, and V. Cardoso, *Destabilizing the Fundamental Mode of Black Holes: The Elephant and the Flea*, *Phys. Rev. Lett.* **128**, 111103 (2022), [[2111.05415](#)].
- [42] B. Wang, C.-Y. Lin, and C. Molina, *Quasinormal behavior of massless scalar field perturbation in Reissner-Nordstrom anti-de Sitter spacetimes*, *Phys. Rev. D* **70**, 064025 (2004), [[hep-th/0407024](#)].
- [43] J. L. Blázquez-Salcedo, C. F. B. Macedo, V. Cardoso, V. Ferrari, and L. Gualtieri, *Perturbed black holes in Einstein-dilaton-Gauss-Bonnet gravity: Stability, ringdown, and gravitational-wave emission*, *Phys. Rev. D* **94**, 104024 (2016), [[1609.01286](#)].
- [44] G. Franciolini, L. Hui, R. Penco, L. Santoni, and E. Trincherini, *Effective Field Theory of Black Hole Quasinormal Modes in Scalar-Tensor Theories*, *JHEP* **02**, 127 (2019), [[1810.07706](#)].
- [45] A. Aragón, P. A. González, E. Papantonopoulos, V. Ferrari, and Y. Vásquez, *Quasinormal modes and their anomalous behavior for black holes in  $f(R)$  gravity*, *Eur. Phys. J. C* **81**, 407 (2021), [[2005.11179](#)].
- [46] H. Liu, P. Liu, Y.-Q. Liu, B. Wang, and J.-P. Wu, *Echoes from phantom wormholes*, *Phys. Rev. D* **103**, 024006 (2021), [[2007.09078](#)].
- [47] T. Karakasis, E. Papantonopoulos, and C. Vlachos,  *$f(R)$  gravity wormholes sourced by a phantom scalar field*, *Phys. Rev. D* **105**, 024006 (2022), [[2107.09713](#)].
- [48] P. A. Cano, K. Fransen, T. Hertog, and S. Maenaut, *Gravitational ringing of rotating black holes in higher-derivative gravity*, *Phys. Rev. D* **105**, 024064 (2022), [[2110.11378](#)].
- [49] P. A. González, E. Papantonopoulos, J. Saavedra, and Y. Vásquez, *Quasinormal modes for massive charged scalar fields in Reissner-Nordström dS black holes: anomalous decay rate*, [[2204.01570](#)].
- [50] Y. Zhao, R. Xin, A. Ilyas, E. N. Saridakis, and Y.-F. Cai, *Quasinormal modes of black holes in  $f(T)$  gravity*, [[2204.11169](#)].
- [51] A. Ishibashi and H. Kodama, *Stability of higher dimensional Schwarzschild black holes*, *Prog. Theor. Phys* **110**, 901 (2003), [[hep-th/0305185](#)].
- [52] A. Chowdhury, S. Devi, and S. Chakrabarti, *Naked singularity in 4D Einstein-Gauss-Bonnet novel gravity: Echoes and (in)-stability*, [[2202.13698](#)].
- [53] K. Kristensen, R.-C. Ge, and S. Hughes, *Normalization of quasinormal modes in leaky optical cavities and plasmonic resonators*, *Phys. Rev. A* **92**, 053810 (2015), [[1501.05938](#)].
- [54] S. S. Seahra, *Ringling the Randall-Sundrum braneworld: Metastable gravity wave bound states*, *Phys. Rev. D* **72**, 066002 (2005), [[hep-th/0501175](#)].
- [55] S. S. Seahra, *Metastable massive gravitons from an infinite extra dimension*, *Int. J. Mod. Phys. D* **14**, 2279 (2005), [[hep-th/0505196](#)].
- [56] Q. Tan, W.-D. Guo, and Y.-X. Liu, *Sound from extra dimension: quasinormal modes of thick brane*, [[2205.05255](#)].
- [57] Y.-F. Cai, G. Cheng, J. Liu, M. Wang, and H. Zhang, *Features and stability analysis of non-Schwarzschild black hole in quadratic gravity*, *JHEP* **01**, 108 (2016), [[1508.04776](#)].
- [58] V. Cardoso, M. Kimura, A. Maselli, E. Berti, and C. F. B. Macedo, *Parametrized black hole quasinormal ringdown: Decoupled equations for nonrotating black holes*, *Phys. Rev. D* **99**, 104077 (2019), [[1901.01265](#)].
- [59] R. McManus, E. Berti, C. F. B. Macedo, M. Kimura, A. Maselli, and V. Cardoso, *Parametrized black hole quasinormal ringdown. II. Coupled equations and quadratic corrections for nonrotating black holes*, *Phys. Rev. D* **100**, 044061 (2019), [[1906.05155](#)].

- [60] V. Cardoso, W.-D. Guo, C. F. B. Macedo, and P. Pani, *The tune of the Universe: the role of plasma in tests of strong-field gravity*, *Mon. Not. Roy. Astron. Soc.* **503**, 563 (2021), [[2009.07287](#)].
- [61] Y. Hatsuda, *Quasinormal modes of Kerr-de Sitter black holes via the Heun function*, *Class. Quant. Grav.* **38**, 025015 (2020), [[2006.08957](#)].
- [62] S. Noda and H. Motohashi, *Spectroscopy of Kerr-AdS5 spacetime with the Heun function: Quasinormal modes, greybody factor, and evaporation*, *Phys. Rev. D* **106**, 064025 (2022), [[2206.07721](#)].
- [63] G. Guo, P. Wang, H. Wu and H. Yang, *Quasinormal Modes of Black Holes with Multiple Photon Spheres*, [[2112.14133](#)].
- [64] S. Stotyn and R. B. Mann, *Magnetic charge can locally stabilize kaluza-klein bubbles*, *Phys. Lett. B* **705**, 269 (2011), [[1105.1854](#)].
- [65] Y.-X. Liu, *Introduction to Extra Dimensions and Thick Braneworlds*, [[1707.08541](#)].
- [66] R. Gregory, and R. Laflamme, *Black strings and p-branes are unstable*, *Phys. Rev. Lett.* **70**, 2837 (1993), [[hep-th/9301052](#)].
- [67] D. Ghosh, A. Thalappilil and F. Ullah, *Astrophysical hints for magnetic black holes*, *Phys. Rev. D* **103**, 023006 (2021), [[hep-th/2009.03363](#)].
- [68] M. D. Diamond and D. E. Kaplan, *Constraints on relic magnetic black holes*, *JHEP* **03**, 157 (2022), [[2103.01850](#)].
- [69] V. Karas and Z. Stuchlik, *Magnetized black holes: interplay between charge and rotation*, *Universe* **9**, 267 (2023), [[2306.07804](#)].
- [70] J. A. Wheeler, *Geometrodynamics*, (New York, 1973).
- [71] A. R. Ruffini, *Black Holes: les Astres Occlus*, (Gordon and Breach Science Publishers, New York, 1973).
- [72] A. R. Ruffini, *Angular momentum in quantum mechanics*, (Princeton University Press, Princeton, 1996).
- [73] T. Regge and J. A. Wheeler, *Stability of a Schwarzschild Singularity*, *Phys. Rev.* **108**, 1063 (1957).
- [74] S. Chandrasekhar, *The Mathematical Theory of Black Holes*, (Oxford University Press, New York, 1983).
- [75] H. Ciftci, R. L. Hall, and N. Saad, *Perturbation theory in a framework of iteration methods*, *Phys. Lett. A* **340**, 388 (2005), [[math-ph/0504056](#)].
- [76] H.-T. Cho, A. S. Cornell, J. Doukas, T.-R. Huang, and W. Naylor, *A New Approach to Black Hole Quasi-normal Modes: A Review of the Asymptotic Iteration Method*, *Adv. Math. Phys.* **2012**, 281705 (2012), [[1111.5024](#)].